Impedimetric Toxicity Assay in Microfluidics Using Free and Liposome-Encapsulated Anticancer Drugs

Claudia Caviglia,[†] Kinga Zór,[†] Lucia Montini,[†,‡,⊥] Valeria Tilli,[†,‡,⊥] Silvia Canepa,[†] Fredrik Melander,[†] Haseena B. Muhammad,[†] Marco Carminati,[§] Giorgio Ferrari,[§] Roberto Raiteri,[∥] Arto Heiskanen,[†] Thomas L. Andresen,[†] and Jenny Emnéus*[,†]

[†]Department of Micro- and Nanotechnology, Technical University of Denmark, DK-2800 Kongens Lyngby, Denmark

[‡]Section of Pharmaceutical Biology, University of Siena, I-53100 Siena, Italy

[§]Dipartimento di Elettronica, Informazione e Bioingegneria, Politecnico di Milano, I-20133 Milan, Italy

[∥]Department of Informatics, Bioengineering, Robotics, and System Engineering, University of Genova, I-16145 Genova, Italy

Received: September 26, 2014
Accepted: January 12, 2015
Published: January 12, 2015

Corresponding Author

*Phone: +45 45 25 68 67. Fax: +45 45 88 77 62. E-mail: jenny.emneus@nanotech.dtu.dk.

Author Contributions

[⊥]L.M. and V.T. contributed equally to this work.

Cancer has become the leading cause of death in many countries,[1] with chemotherapy representing one of the most important treatment strategies.[2] To improve the success rate of chemotherapy, targeted drug delivery systems (TDDS) are being developed where tumor targeting vehicles transport anticancer drugs to the tumor site, increasing drug accumulation in cancer cells.[3] TDDS are aimed to avoid damage in healthy cells and increase the efficiency of the drug in cancer cells. Liposomal TDDS have been in focus of anticancer drug development during the last 40 years exploiting the biochemical differences between healthy and cancer cells (pH- and enzyme-triggered release, etc.).[4,5] Understanding the influence of a drug or a treatment on a multitude of cellular events, such as changes in adhesion, morphology, proliferation, metabolism, communication, and ultimately cell death, is fundamental for research in drug discovery.[6] Therefore, in parallel with the development and screening of drug candidates and novel TDDS, there is a demand for exploring new ways to study dynamic cellular processes that regulate the behavior of cancer cells[7] and the interaction of cells with drugs and TDDS.

Cell-based assays are widely used for screening and validation of drug candidates as well as for toxicity testing in preclinical studies.[6,8] The effects of drugs on specific cellular properties are usually evaluated by in vitro cell-based experiments that assess cell number and viability/cytotoxicity using, e.g., Alamar Blue, MTS (3-(4,5-dimethylthiazol-2-yl)-5-(3-carboxymethoxyphenyl)-2-(4-sulfophenyl)-2*H*-tetrazolium), neutral red uptake, ATP, and lactate dehydrogenase, as well as growth (e.g., colony forming efficiency), migration, and adhesion assays.[6,8−13] Many of these assays are, however, based on single end point measurements, performed on individual cell populations without providing real-time insight about the kinetics of the biological event of interest. Moreover, aside from being labor intensive and resource consuming, most of these conventional assays require multiple additions of chemicals and labeling steps that can interfere or disrupt cellular functions

making them invasive. To better understand the mechanisms of action and effect that drugs exert on cell populations, there is a need to develop and explore complementary methods that are label-free, minimally invasive, and capable of continuous real-time monitoring of biological events in vitro.[14,15]

The development of cell-based label-free technology has become increasingly attractive for implementation in cell biology and drug discovery.[16] Since one of the consequences of cell death is related to changes in the morphological properties as well as cell−surface and cell−cell adhesion, a number of label-free techniques have emerged, capable of quantitatively determining the cell−substrate interactions in a minimally invasive and real-time manner. This includes electrochemical impedance spectroscopy (EIS), quartz crystal microbalance, refractive index based technologies, and optical waveguide light mode spectroscopy.[14,16] Among these techniques, impedance-based measurements, first presented by Giaever and Keese in 1984,[17] rely on the insulating properties of adhering cells, which affect the ionic environment at the electrode/electrolyte interface. Impedance-based methods have been developed and successfully applied for monitoring cell adhesion and spreading,[18] motility,[19] proliferation, and cytotoxicity.[20−25] EIS-based assays provide distinct quantitative information about the kinetics of cellular behavior, enabling real-time monitoring of cellular dynamics of the same cell population over several days. This technique has gained increasing attention in evaluating the behavior of cancer cells and the effects of different anticancer drugs.[22,24,26−35]

Since its introduction, the concept of micro total analysis systems (μTAS)[36] has been adopted for cell-based drug screening performed in microfluidic perfusion culture systems,[37−39] providing a steady controllable and more in vivo-like microenvironment. Perfusion culture diminishes the limitations of static culture systems, i.e., risk of contamination during long-term culturing, environmental fluctuations due to depletion of nutrients, and accumulation of waste products, and enables a more reliable and reproducible evaluation of the drug-induced cellular responses.[40] EIS-based detection has been widely used to monitor cell cultures under static conditions.[21,23,27,35,41] However, systems that combine the advantages of perfusion cell culture with label-free electrochemical and optical detection for multiparameter analysis are an emerging field of research.[32,33,42−45]

The here-presented compact microfluidic cell culture and electrochemical analysis platform with in-built fluid handling and detection[46,47] represents an improvement to the existing μTAS devices where the down-scaling of the liquid handling and electrochemical detection is often overlooked. The platform enables parallel EIS measurements and optical detection for real-time monitoring and evaluation of cellular responses to different anticancer drugs and TDDS in four independent culture chambers, each containing three independent electrode arrays. We studied the time-dependent cytotoxic effects of different concentrations of doxorubicin (DOX), a well-known chemotherapeutic drug,[48] on HeLa cells. The obtained results were compared with data from our previous studies performed under the same conditions in static environment.[49] The assessment of the differences/similarities between static and microfluidic conditions is significant given the recent popularity of microfluidic cytotoxicity assays and the lack of comparative studies. The cytotoxic response induced by free and liposome-encapsulated OX on a fibrosarcoma cell line (HT1080) and a laryngopharynx carcinoma cell line (FaDu) was also evaluated.

In addition, the potential for optical detection was demonstrated with the annexin V/propidium iodide (ANNV/PI) assay for apoptosis, complementary to EIS monitoring of the DOX effect on HeLa cells. Moreover, the time-dependent response of HeLa cells to DOX-induced cytotoxicity was compared with the response obtained using oxaliplatin (OX), another widely used anticancer drug.[50,51]

MATERIALS AND METHODS

Chemicals. Sodium hydroxide, potassium hydroxide, hydrogen peroxide, cell culture tested phosphate-buffered saline (PBS), sodium chloride, laminin from Engelbreth−Holm−Swarm murine sarcoma basement membrane, fetal bovine serum (FBS), doxorubicin hydrochloride (DOX), and oxaliplatin (OX) were purchased from Sigma-Aldrich Corporation (St. Louis, MO, U.S.A.). Dulbecco's modified Eagle's medium (DMEM), trypsin−EDTA (0.05%), and penicillin/streptomycin (P/S) were purchased from Life Technologies Ltd. (Paisley, U.K.). Annexin V: FITC apoptosis detection kit I was purchased from BD Biosciences (San Jose, CA, U.S.A.).

Experimental Setup. The microfluidic cell culture and analysis platform, from here on referred to as the EXCELL platform, is designed for real-time monitoring of cellular dynamics[46,47] based on the Mainstream component concept.[52] The composition and function of the fully integrated platform (Figure 1A) has been previously presented.[47]

Briefly, the platform consists of a base plate accommodating the necessary components, such as (1) four peristaltic micropumps with poly(dimethylsiloxane) (PDMS) ribbons[53] operated with Lego interactive servo motors connected to NXT Intelligent Brick units (Lego Systems A/S, Billund, Denmark) controlled by the LabView-based EXCELL software, (2) four sample and/or waste reservoirs (Figure 1C), (3) a "plug-in" microfluidic chip with integrated 12-microelectrode array chip, and (4) the EXCELL potentiostat with a window for microscopic observations (Figure 1A inset) operated by custom-made EXCELL acquisition and analysis software.[45] The data acquisition was done through a portable NI-6259 USB system (National Instruments Corporation, Austin, TX, U.S.A.).

To avoid bubble formation, pressurization of the platform was achieved through a closed-loop gas connection (0.4 bar overpressure of gas mixture composed of 5% CO_2/20% oxygen/75% nitrogen supplied by AGA A/S, Copenhagen, Denmark) integrated on the lid of inlet and outlet reservoirs (Figure 1C). A filter unit (0.5 μm cutoff) was integrated at each gas connection to avoid contamination and infection during perfusion culture.

The cell culture/detection unit (Figure 1D) is formed by integration of the "plug-in" microfluidic chip with the microelectrode array chip fabricated using standard lithography according to previously established protocol.[46,47,54] The integration is achieved by placing the microelectrode chip in a 5 mm poly(methyl methacrylate) (PMMA) holder, which is attached to the microfluidic chip using a silicon adhesive gasket (INT TA106) (Intertronics, Oxfordshire, U.K.) cut using laser ablation.[47] The microfluidic chip is composed of three 500 μm thick micromilled PMMA layers, bonded together using previously established UV-assisted thermal bonding method.[47] The cell culture/detection unit comprises four microfluidic chambers (internal volume of approximately 2 μL), schemati-

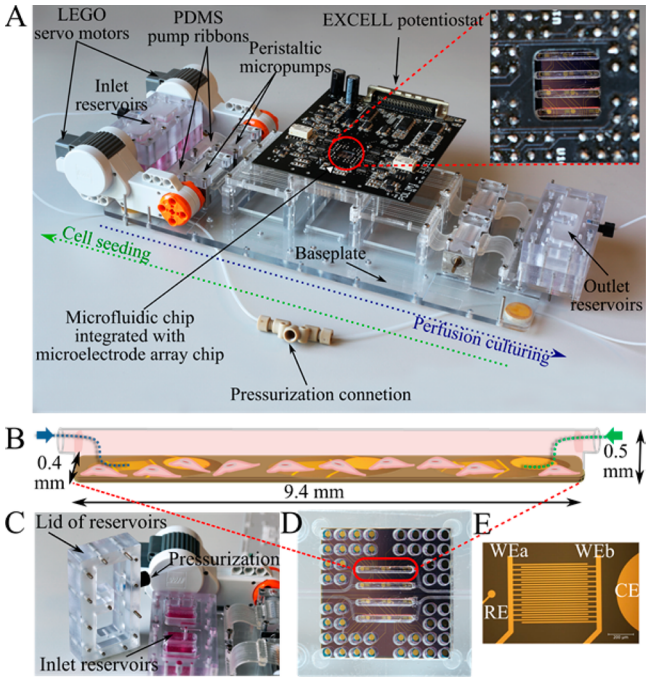

Figure 1. EXCELL platform. (A) Photograph of the fully integrated platform showing its main components, including the EXCELL potentiostat with a window for microscopic observations (inset). Green and blue arrows indicate the flow direction used for cell seeding and perfusion culturing, respectively. (B) Schematic representation of an individual microfluidic chamber in the cell culture/detection unit containing three electrode arrays. (C) Photograph of the reservoirs, showing the lid embedding the gas connection used for pressurization. (D) Photograph of the microfluidic cell culture/detection unit consisting of microfluidic chip integrated with a 12-microelectrode array chip. (E) Microscopic image of a single electrode array showing the counter (CE), reference (RE), and working (WEa and WEb) electrodes.

cally presented in Figure 1B, each having three electrode arrays [counter (CE), reference (RE), and interdigitated working electrode (WEa and WEb)] (Figure 1E). Each of the two sides of the interdigitated electrodes (IDE) is independently addressable and composed of 12 digits (length, 500 μm; width and gap, 10 μm). Prior to integration, the microelectrode chip was chemically cleaned (25% H_2O_2/50 mM KOH for 10 min) to obtain reliable and reproducible measurements between the electrodes.[55]

Cell Seeding and Culture. HeLa (cat. 85060701) and HT1080 (cat. 85111505) cells were purchased from Sigma-Aldrich Corporation (St. Louis, MO, U.S.A.) and FaDu cells (ATCC HTB-43) from ATCC (Wesel, Germany). In preparation for experiments, cells were cultured in standard T25 flasks with medium exchange regularly every 2 days. Cell suspensions were prepared after standard trypsinization using trypsin−EDTA solution. Cells were centrifuged for 5 min at 900 rpm at 20 °C and then resuspended in cell culture medium. The cell number was determined using a hemacytometer, and the desired cell densities were prepared by diluting the initially prepared cell suspension with fresh culture medium. Cells were cultured in DMEM supplemented with 10% FBS and 1% P/S in an ordinary humidified incubator at 37 °C (5% CO_2 in air).

Prior to cell seeding in microfluidics, the electrodes were electrochemically cleaned online by linear potential sweep from −200 to −1200 mV at 50 mV/s scan rate in 50 mM KOH.[55] Before starting the cell-based assay, the platform was sterilized following a previously described procedure[47] by flushing the channels and the chambers with 500 mM NaOH solution (5 μL/min for 20 min), followed by rinsing with PBS (15 μL/min for 30 min). The sterilization was followed by an online surface coating with laminin (20 μg/mL, 2 h, 37 °C, 250 nL/min) under pressurization followed by rinsing with PBS (5 μL/min for 15 min). Cell seeding in microfluidics was performed under pressurization applying reverse flow (7 μL/min for 15 min) from the outlet reservoirs toward the inlets. This strategy was chosen to (i) eliminate any possible mechanical cell damage caused by the peristaltic micropumps and (ii) minimize the number of cells that sediment and adhere in the upstream microfluidic channels and inlet reservoirs as previously described by Zór et al.[47] The progress of cell seeding was continuously monitored under a microscope. In order to facilitate cell attachment, cell seeding was followed by a 1 h incubation step (37 °C, 5% CO_2, 95% air) at stopped-flow condition. After seeding, both inlet and outlet vials were thoroughly rinsed to remove the remaining cells and filled with fresh culture medium followed by perfusion culturing (250 nL/min) under pressurization.

At the end of each experiment cells were removed by perfusing 500 mM NaOH at 30 μL/min for 15 min, followed by 15 min rinsing with PBS. The microelectrode array, integrated with the microfluidic cell culture chip, was regenerated by electrochemical cleaning, as described above.

Microfluidic Cytotoxicity Assays. *EIS-Based Cytotoxicity Assay.* EIS monitoring of drug-induced cell death was performed by seeding HeLa cells in the four microfluidic chambers on laminin-coated electrode arrays at a density of 280 cells/WE (100 000 cells/cm^2). Cells were cultured under perfusion conditions (the flow was directed from the inlet reservoirs toward the outlets) for approximately 20 h followed by medium exchange with fresh medium containing the desired concentration of the anticancer drug. Simultaneously, three DOX concentrations were introduced (2.5, 5, and 100 μM). In experiments with OX, the used concentrations were 100 and 500 μM. After the drug addition, the reservoirs were closed (pressurization re-established) and the system was placed inside the incubator for EIS monitoring under continuous flow (250 nL/min). EIS monitoring of cell death induced by OX-loaded liposomes was performed using HT1080 and FaDu cells seeded in the microfluidic chambers with laminin-coated electrodes at a density of 150 cells/WE (60 000 cells/cm^2). Cells were cultured for 40 h and then, following the procedure described above, the medium in the reservoirs was replaced by fresh medium containing the drug-loaded liposomes. For all experiments, at least one chamber was continuously perfused with drug-free culture medium and used as control.

EIS recordings were performed continuously at a time interval of 1 h over the entire experimental period from cell seeding to the end of an assay. The applied sinusoidal perturbation potential was set to 200 μV, and full spectra were acquired in the frequency range from 100 Hz to 100 kHz measuring 10 data points/decade with an averaging time of 2 s per point. Measurements were performed using the coplanar interdigitated sensing configuration.[56] Bright-field images were acquired using a Zeiss AxioImager M1m microscope (Carl Zeiss AG, Göttingen, Germany) equipped with a Neo 5.5 sCMOS camera under control of Solis (i) software (version 4.22.30007.0) from Andor Technology Ltd. (Belfast, U.K.).

Changes in impedance magnitude were expressed using the dimensionless parameter Cell Index,[24] which represents the maximum value of normalized impedance. For each time point, Cell Index is calculated as

$$\text{Cell Index}(t) = \max_{i=1,\ldots,N} \frac{|Z(t, f_i)| - |Z(0, f_i)|}{|Z(0, f_i)|} \quad (1)$$

where $|Z(t,f_i)|$ is the magnitude of the impedance at a given time and frequency, $|Z(0,f_i)|$ is the magnitude of the impedance at the same frequency recorded in the absence of cells at the beginning of the experiment, and N is the number of frequency points at which the impedance is recorded. In our work, for each time point, the Cell Index was calculated analyzing the entire spectrum ($N = 30$). Data were processed using an ad-hoc algorithm implemented in Matlab (R2013a), while Origin (version 9.0) was used for data plotting.

In order to quantify the time dependency of cytotoxicity we have defined the half-maximal inhibitory time (IT50)[49] (eq 2), analogous to the IC50, as a quantitative measure to indicate how long time is required for the drug to cause 50% decrease in cell viability. The sigmoidal fitting of the data and the IT50 values were calculated using the logistic four-parameter function [Origin (version 9.0)]

$$y = \frac{\text{Cell Index}_{\text{initial}} - \text{Cell Index}_{\text{final}}}{1 + (t/\text{IT50})^p} + \text{Cell Index}_{\text{final}} \quad (2)$$

where t is time and p is the slope. Correspondingly, the presented values of IT20 and IT80 were calculated using eq 2.

Fluorescence-Based Cytotoxicity Assay. Annexin V/propidium iodide end point staining was performed online during DOX-induced cytotoxicity by introducing the same DOX concentrations as for EIS-based assays. HeLa cells were seeded in the microfluidic chambers at a density of 280 cells/WE (100 000 cells/cm^2) as for EIS-based cytotoxicity assays. Thirty-eight hours after drug addition the experiment was stopped and the staining performed. Cells were washed by perfusing PBS at a flow rate of 5 μL/min for 30 min, followed by 15 min of perfusion with binding buffer provided in the kit. Then, annexin V/PI was introduced and perfusion was continued for 30 min. During the required steps for staining, the platform was kept in the incubator. The staining was terminated by 15 min perfusion with the binding buffer followed by fluorescence imaging. The perfusion times with the dyes include also the time required for the solutions in the inlet reservoirs to reach and fill the microfluidic culture chambers (10 min).

RESULTS AND DISCUSSION

Cytotoxic Effects of DOX and OX on HeLa Cells.

Optimization of Cell Seeding Density. When seeding cells in microfluidic systems, one of the major challenges is controlling the initial cell density,[57] especially the number of cells on the WE.[47] Since an EIS-based assay relies on and responds to cell−electrode interactions, for the accuracy of the assay a reproducible and uniform cell distribution is a mandatory prerequisite. Cell suspensions with several densities of HeLa cells (1×10^6, 2×10^6, 3×10^6, 5×10^6, 8×10^6, 10^7 cells/mL) were prepared in culture medium, placed in the outlet reservoirs, and seeded in the culture chambers to define the optimum cell density for the toxicity assay.

Microscopic images were acquired, and the number of cells sedimented on the WEs was quantified. Figure 2A shows the

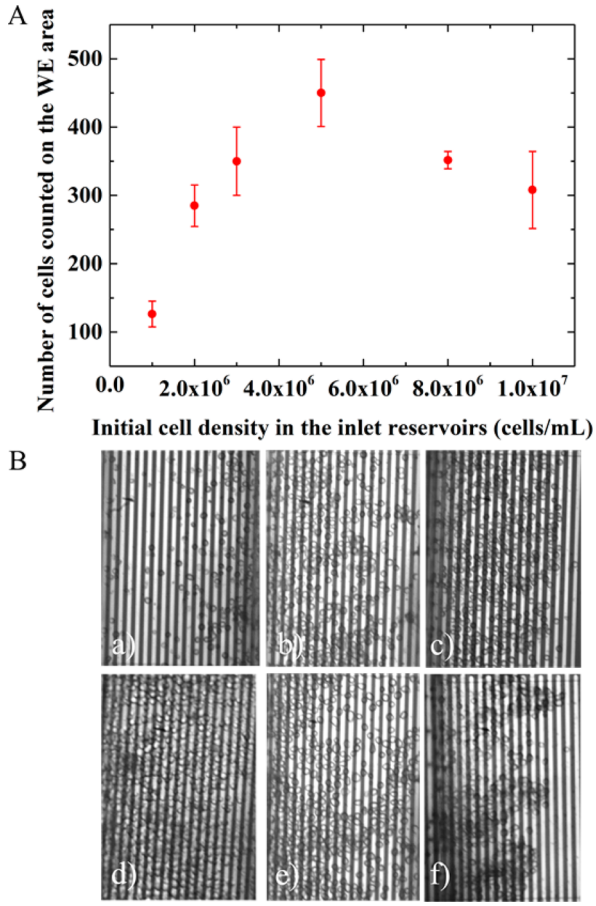

Figure 2. (A) Correlation between initial HeLa cell density placed in the outlet reservoirs (1×10^6, 2×10^6, 3×10^6, 5×10^6, 8×10^6, 10^7 cells/mL) and number of cells counted on the WE area after seeding. Error bars represent standard deviation, $n = 6$. (B) Representative microscopic images of HeLa cells seeded on the WE area using different densities of cells (a) 1×10^6, (b) 2×10^6, (c) 3×10^6, (d) 5×10^6, (e) 8×10^6, (f) 10^7 cells/mL.

relationship between the initial cell density of cell suspensions placed in the outlet reservoirs and the number of cells counted on the WEs. A linear correlation between the cell density in suspension and the number of cells on the WEs (Figure 2A), as well as a uniform cell distribution (Figure 2B), can be observed in the range from 2×10^6 to 5×10^6 cells/mL. Lower (1×10^6) and higher (8×10^6 and 10^7) cell densities resulted in an uneven cell distribution and deviation from the linear correlation. A low cell density in the suspension does not provide a sufficient amount of cells to result in a uniform coverage on the WEs (Figure 2B, panel a), whereas in suspensions with high cell densities cluster formation obstructs the flow in the microchannels affecting the cell distribution on the WEs (Figure 2B, panels e and f).

DOX-Induced Cell Death. DOX acts against a broad range of cancer cells[48] with different proposed mechanisms of action, such as intercalation into DNA during cell division and induction of oxidative stress through free radical formation.[58] On the basis of the performed cell seeding optimization (Figure 2), HeLa cells were seeded on the microelectrode arrays with an initial density of 280 cells/WE (100 000 cells/cm^2). This density was chosen to obtain a cell confluence below 50%, ensuring sufficient space for effective cell proliferation that results in a growth curve characterized by a stable steady state

for the entire experimental period as previously shown for assays under static conditions.[49]

Cells were first cultured under perfusion conditions for 20 h, and then fresh medium, containing 2.5, 5, and 100 μM DOX, was introduced in three of the cell culture chambers. Figure 3A shows the real-time kinetic responses of HeLa cells to the different DOX concentrations (presented as relative Cell Index, 100% indicating the value for each population before introduction of DOX). The bar graph in Figure 3B shows the Cell Index % related to different time points (5, 10, 20, 30, 40, and 50 h after the drug addition) for each DOX concentration. While 100 μM induces fast cell death, 2.5 and 5 μM result in slower cytotoxic responses. The curve related to 2.5 μM shows an initial Cell Index increase, which after 20 h is followed by a slow decrease down to 0. In our previous study, performed using the same microelectrode array chip under static conditions,[49] the initial increase in Cell Index was also observed; however, its manifestation was more pronounced. This is attributed to the intensified metabolic activity of the cells and probably changes in cell morphology and adhesion properties in response to the stress when trying to overcome the apoptosis induced by accumulation of the drug.[35] In the case of 5 μM DOX, no initial increase in Cell Index was observed as previously reported for assays under static conditions.[49] In contrast, the Cell Index profile of the control shows a steady increase during the entire length of the experiment, necessary to provide proper control conditions in comparison with the drug-treated cell populations.

Among several standard techniques generally used for assessing cell viability/cytotoxicity, optical detection is most widely used in drug screening and cytotoxicity studies.[6,13] Optical techniques can easily be applied in cell-based microfluidic systems[8,59] and coupled to other detection techniques providing multiparameter high-content assays. In this study, the effects of DOX on HeLa cell populations were also evaluated using the fluorescence microscopy based ANNV/PI assay adapted to microfluidics as an online end point method complementary to the performed EIS-based assays under the same conditions. The ANNV/PI assay was performed 38 h after DOX introduction using the initial cell density of 100 000 cells/cm^2. Figure 3C shows fluorescence microscopic images of the cells influenced by the different drug concentrations. PI (red) stains the cells that have lost the integrity of their plasma and nuclear membranes (late apoptotic and necrotic cells). ANNV (green) binds to plasma membrane located phosphatidylserines that in apoptotic cells are oriented toward the extracellular environment. In viable cells, they are exposed on the intracellular side of the plasma membrane. Therefore, using the combination of ANNV and PI, it is possible to distinguish between early (ANNV$^+$/PI$^-$) and late apoptotic cells (ANNV$^+$/PI$^+$), as well as necrotic (ANNV$^-$/PI$^+$) and viable cells (ANNV$^-$/PI$^-$). In the case of 5 μM DOX, panels a and d of Figure 3C indicate that most of the cells had detached from the electrode surfaces due to complete cell death, and among the remaining cells the majority showed early apoptotic stage (ANNV$^+$/PI$^-$). This is in accordance with the EIS-based assay, which at this time point showed low Cell Index % value ($\leq$10%), reflecting both complete detachment of dead cells and lowered adhesion of the remaining cells. On the other hand, the majority of the cells exposed to 2.5 μM DOX were still adhered on the electrode surface, only some showing fluorescence as an indication of drug-induced apoptosis (Figure 3C, panels b and e). Among the fluorescing cells, a majority

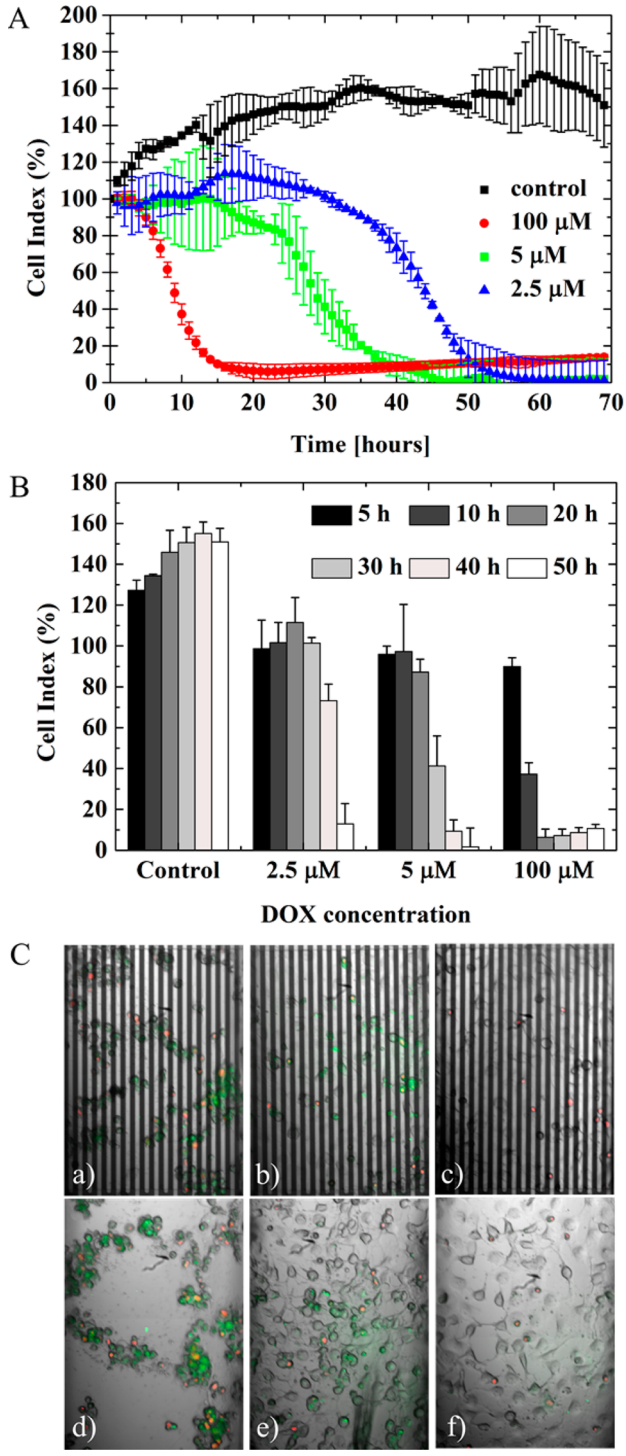

Figure 3. (A) Representative Cell Index (%) profiles showing real-time kinetics of DOX-induced cell death: HeLa cells were seeded in the cell culture chambers (100 000 cells/cm^2) and DOX was introduced 20 h after cell seeding (t = 0) at a final concentration of 2.5, 5, and 100 μM (100% Cell Index indicates the value for each cell population at t = 0). (B) Bar diagram showing Cell Index (%) at 5, 10, 20, 30, 40, and 50 h after introduction of different DOX concentrations. (C) Representative fluorescence microscopic images of HeLa cells after performing the ANNV/PI assay: images showing cells on the WE (a–c) and CE area (d–f). The fluorescence-based assay was performed online 38 h after introduction of DOX at different concentrations [(a and d) 5 μM, (b and e) 2.5 μM, (c and f) no drug]. Error bars represent standard deviation, n = 3.

were stained green ($ANNV^+/PI^-$), indicating early apoptosis. Cells exposed to 100 μM DOX completely lost their adherence on the electrodes and were flushed away from the microfluidic chamber (images not shown). The cells in the control chamber remained viable (Figure 3C, panels c and f).

Evaluation of Cell Death Rate: Comparison between Perfusion Culture and Static Conditions. The comparison between the cytotoxic effect of DOX on HeLa cells in perfusion culture and under static conditions based on our previous study using the same microelectrode array chip[49] was made using the calculated IT50 values.[49] We found that, under static conditions, the IT50 for 2.5, 5, and 100 μM was lower (11.6, 5.1, and 3.3 h, respectively) than the corresponding IT50 in perfusion culture (43.2, 29.5, and 8.2 h, respectively) (Figure 4).

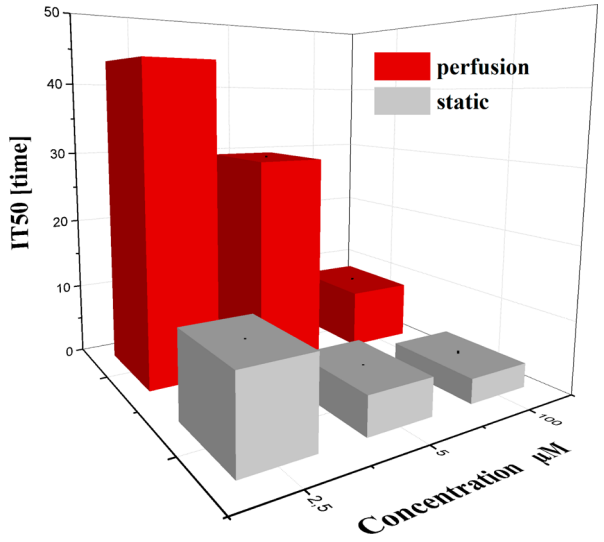

Figure 4. Evaluation of the inhibitory time (IT) upon introduction of 2.5, 5, and 100 μM DOX: the bars show the time required for 50% (IT50) decrease in HeLa cell viability in static and perfusion cultures. Error bars represent standard deviation, n = 3.

These differences could be due to similar factors as previously reported based on observations using colorimetric assays. These reports indicated that there was a substantial difference between static (macro) and microfluidic perfusion culture influencing cell proliferation rate,[40] as well as the response of different cells to the cytotoxic agent 5-fluorouracil.[60]

OX-Induced Cell Death. OX, a third-generation platinum anticancer compound,[61] has shown potential in treating a wide range of cancers both in vitro and in vivo.[62,63] In clinical applications, it is used as a chemotherapeutic agent for treating colorectal cancer.[64] Among the several mechanisms of action proposed for OX, the mainly accepted one is related to the cytotoxic effects induced by DNA damage, resulting in cell growth inhibition and apoptosis.[65] The cytotoxic effect of OX on HeLa cells cultured under perfusion conditions was evaluated using the EIS-based assay and compared with the effect on cell viability induced by DOX. HeLa cells, seeded with an initial density of 280 cells/WE (100 000 cells/cm^2), were cultured for 20 h in the microfluidic platform, after which fresh medium containing 100 μM OX (concentration chosen based on MTS assay shown in the Supporting Information Figure S1) was introduced. A control experiment was performed in parallel in drug-free medium. Figure 5 shows the comparison of real-time cytotoxic responses of HeLa cells to DOX and OX and the calculated IT (20, 50, and 80) values.

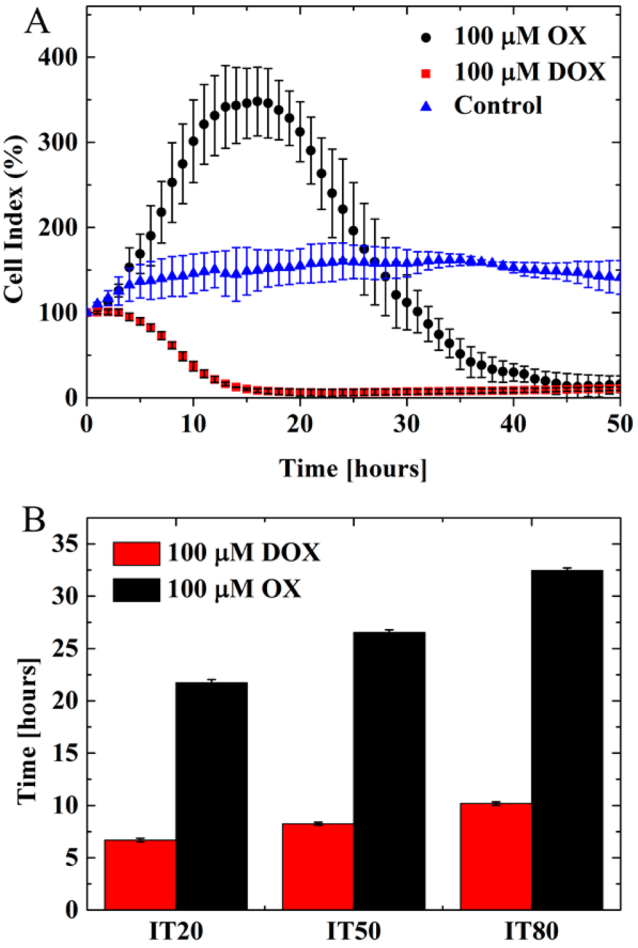

Figure 5. (A) Representative Cell Index (%) profiles of drug-induced HeLa cell death: HeLa cells were seeded (100 000 cells/cm^2) and grown in the microfluidic platform, and the drugs (100 μM DOX and 100 μM OX) were added 20 h after cell seeding (t = 0). Error bars represent standard deviation, n = 3. (B) IT20, IT50, and IT80 values for HeLa cells treated with 100 μM DOX and 100 μM OX. Error bars represent standard deviation, n = 3.

The Cell Index profiles show that 100 μM OX induces a slower response compared to the same concentration of DOX. The difference in the response time is mainly due to the OX-induced initial increase in Cell Index up to 350% during 18 h prior to the onset of cell death indicated by the strong decrease in Cell Index. Introduction of 500 μM OX results in a corresponding increase in Cell Index; however, due to the increased cytotoxic effect, the observed Cell Index increase has a significantly shorter duration and lower magnitude (Supporting Information Figure S2). This behavior, previously observed in EIS-based assays using other drugs or cell lines, has been attributed to drug-induced stress, which cells try to overcome by increasing their metabolism[30,42,49] or changing their morphology and adhesion.[49] When comparing these data with results obtained in MTS assays performed at different time points with the same cell density and drug concentration, a weak increase in cellular metabolism can be observed upon introduction of OX (Supporting Information Figure S3). This

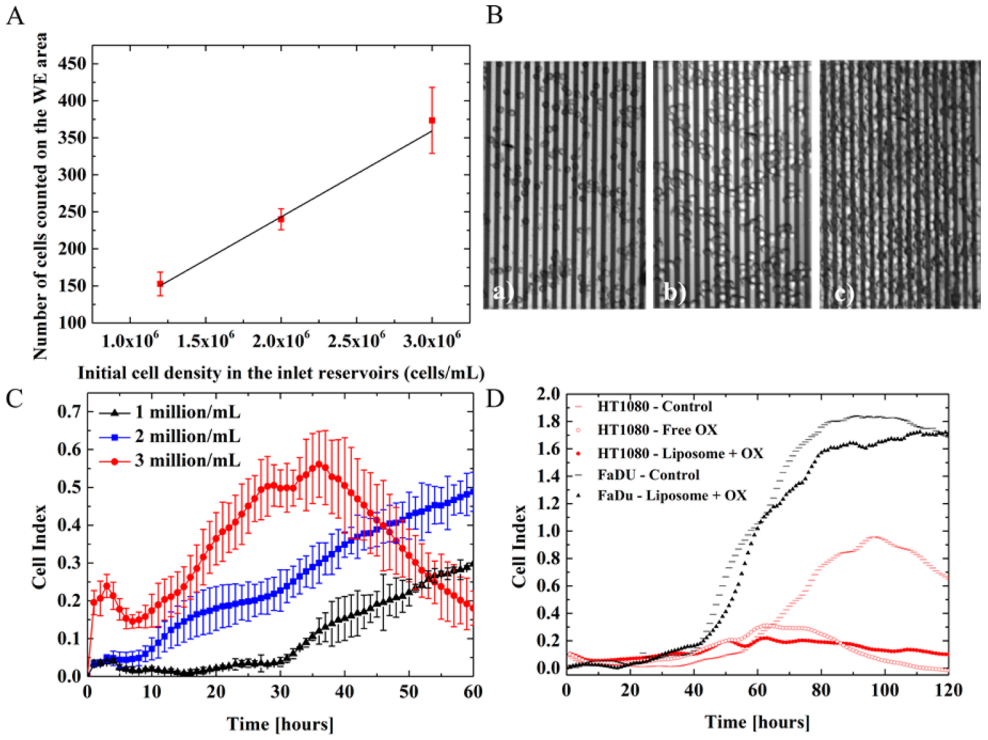

Figure 6. (A) Correlation between initial cell density of HT1080 cells placed in the inlet reservoirs (1.2×10^6, 2×10^6, 3×10^6 cells/mL) and number of cells counted on the WE area after perfusion seeding. Error bars represents standard deviation, $n = 6$. (B) Representative microscopic images of HT1080 cells seeded on the WE area using different initial cell densities (a) 1.2×10^6, (b) 2×10^6, (c) 3×10^6 cells/mL. (C) Cell Index vs time for real-time EIS monitoring of HT1080 cell adhesion and proliferation over 60 h. Cells were initially seeded at different densities (1.2×10^6, 2×10^6, 3×10^6 cells/mL). Error bars represents standard deviation, $n = 3$. (D) Cell Index vs time of drug-induced cell death studied on HT1080 and FaDu cells. Cells were seeded (60 000 cells/cm^2), cultured for 40 h, and exposed to 25 μM free OX or 25 μM OX loaded in liposomes. The Cell Index time dependency curves show the cell viability changes from the beginning of the experiment (cell seeding, $t = 0$).

comparison between EIS-based and MTS assay indicates that the cellular response before the onset of cell death is more related to changes in cell morphology and adhesion, which are monitored by EIS. In the control experiments, a slight increase in Cell Index due to continued proliferation could be observed until a plateau is reached (100% confluence).

Cytotoxic Effects of Liposome-Encapsulated OX on HT1080 and FaDu Cells. Several different liposomal TDDS have been developed, and various strategies explored, considering specific histological, histochemical, and biochemical properties characteristic of tumor tissues to achieve controlled drug release at a specific tumor site with efficient uptake.[3,66,67] One of the approaches in TDDS development is based on the presence of enzymes which are specifically overexpressed in tumors, such as matrix metalloproteinases (MMPs). This group of extracellularly secreted enzymes is generally involved in the proteolysis of the extracellular matrix proteins and basement membranes. It has been reported that certain MMP subtypes were overexpressed in a wide range of tumors,[68] and cancer cells were found to use proteolysis for invasion and metastasis. Hence, the ability of MMPs to degrade peptides and proteins can be exploited to (1) trigger and control the liposomal drug release if lipopeptides are incorporated into the liposome membrane or (2) cleave off poly(ethylene glycol) (PEG)-modified peptides, increasing the cellular uptake of liposomes. To explore the potential of the EIS-based microfluidic platform, studies were carried out monitoring in real time the response of MMP-triggered activation of a newly developed (unpublished data) liposomal drug delivery formulation. HT1080 fibrosarcoma cells, overexpressing MMPs both in vitro and in vivo,[69] were used as the model cell line, while OX was used as the model drug.

The optimization of cell density was performed as previously described for HeLa cells introducing different densities (1.2×10^6, 2×10^6, 3×10^6 cells/mL) of HT1080 cells and following their proliferation for 60 h. Figure 6A shows the linear correlation between the initial cell density in the inlet reservoirs and the number of cells counted on the WEs, while Figure 6B shows the uniform cell distribution. Figure 6C shows the Cell Index profiles during 60 h related to the adhesion and proliferation of HT1080 cells. Both 1.2×10^6 (150 cells/WE; chosen for the assay) and 2×10^6 cells/mL provide a steadily increasing Cell Index profile suitable for long-term cytotoxicity assays. It can be observed that at high initial cell densities (3×10^6 cells/mL) the complete confluence in the chamber is reached in approximately 35 h (max Cell Index) after which the Cell Index strongly decreases. Such cell density is not suitable for long-term cytotoxicity experiments, since the control has to show a Cell Index steady state for a sufficiently long time period.

After 40 h of culturing, free and liposome-encapsulated OX (25 μM) were introduced in the cell culture chambers, while the other two chambers were used as control. The concentration was chosen based on preliminary MTS assay results (Supporting Information Figure S4). Figure 6D shows the real-time cytotoxic responses of HT1080 cell populations to OX. The control shows an increasing Cell Index profile until reaching 100% confluence after 100 h. When exposed to free OX, the drug induces a fast cell death (100% cell death at 120 h), while the OX-loaded liposomes seem to induce a slower

response (50% cell death at 120 h). This behavior can be explained by a slower release of the drug, possibly due to incomplete cleavage of the PEGylated peptides and thereby a reduced degradation of the liposomes. In addition, the cytotoxic effect of liposome-encapsulated OX was tested using FaDu cells, which do not express MMPs in vitro (unpublished results) and cannot, therefore, trigger the release of OX. This is clearly indicated by the inability of liposome-encapsulated OX to induce cytotoxicity as shown in Figure 6D.

CONCLUSION

We have developed an electrochemical impedance spectroscopic assay for evaluating cytotoxic effects of the anticancer drugs doxorubicin (DOX) and oxaliplatin (OX) as well as OX encapsulated in liposomes using a compact microfluidic cell culture and analysis platform comprising fluid handling and detection. Evaluation of doxorubicin-induced cytotoxicity on HeLa cells at different concentrations showed a significant delay in onset of toxicity in comparison with results obtained in static cell cultures presented in our previous study. The obtained results were supported by the data from a fluorescent apoptosis assay performed in microfluidics, proving the potential of the used microfluidic platform that enables both electrochemical and optical detection. We were able to differentiate between the effect of free and liposome-encapsulated OX on induction of cell death in fibrosarcoma cells (HT1080) that produce matrix metalloproteinases (MMP) needed for degradation of drug-loaded liposomes. The MMP-dependent release of OX from the liposomes was confirmed using laryngopharynx carcinoma cells (FaDu) that do not express MMPs, providing a further demonstration of the potential of the impedance-based assay under perfusion culture conditions. Our results, indicating differences between microfluidic perfusion culture and static conditions, combined with the increasing awareness of possible advantages and popularity of microfluidic cell culture, highlight the necessity of comparative studies for in-depth validation of microfluidic cytotoxicity assays.

ASSOCIATED CONTENT

Supporting Information

Additional information as noted in text. This material is available free of charge via Internet.

AUTHOR INFORMATION

Notes

The authors declare no competing financial interest.

ACKNOWLEDGMENTS

The authors wish to acknowledge Houman Pourhassan and Rasmus Eliasen (Ph.D.) for stimulating discussions and Soléne Cherrè for her help with the fluorescence-based assay. Jesper Scheel is acknowledged for the photographs and Jens Hemmingsen for technical help. The microfluidic platform is the outcome of EU FP7 project EXCELL (NMP4-SL-2008-214706). This work and the Ph.D. fellowship of Claudia Caviglia were financially supported by Department of Micro- and Nanotechnology, Technical University of Denmark.

REFERENCES

(1) Jemal, A.; Bray, F.; Ferlay, J. *Ca—Cancer J. Clin.* **2011**, *61*, 69−90.
(2) Chabner, B. A.; Roberts, T. G. J. *Nat. Rev. Cancer* **2005**, *5*, 65−72.
(3) Allen, T. M.; Cullis, P. R. *Science* **2004**, *303*, 1818−1822.
(4) Danhier, F.; Feron, O.; Préat, V. *J. Controlled Release* **2010**, *148*, 135−146.
(5) Allen, T. M.; Cullis, P. R. *Adv. Drug Delivery Rev.* **2013**, *65*, 36−48.
(6) Niles, A. L.; Moravec, R. A.; Riss, T. L. *Expert Opin. Drug Discovery* **2008**, *3*, 655−669.
(7) Martinez, M. M.; Reif, R. D.; Pappas, D. *Anal. Methods* **2010**, *2*, 996−1004.
(8) Zang, R.; Li, D.; Tang, I. C.; Wang, J.; Yang, S. T. *Int. J. Biotechnol. Wellness Ind.* **2012**, *1*, 31−51.
(9) Mosmann, T. *J. Immunol. Methods* **1983**, *65*, 55−63.
(10) Borenfreund, E.; Babich, H.; Martin-Alguacil, N. *Toxicol. In Vitro* **1988**, *2*, 1−6.
(11) Mueller, H.; Kassack, M. U.; Wiese, M. *J. Biomol. Screening* **2004**, *9*, 506−515.
(12) Kramer, N.; Walzl, A.; Unger, C.; Rosner, M.; Krupitza, G.; Hengstschläger, M.; Dolznig, H. *Mutat. Res.* **2013**, *752*, 10−24.
(13) Jurisic, V.; Bumbasirevic, V. *Arch. Oncol.* **2008**, *16*, 49−54.
(14) Hug, T. S. *Assay Drug Dev. Technol.* **2003**, *1*, 479−488.
(15) Pancrazio, J. J.; Whelan, J. P.; Borkholder, D. A.; Ma, W.; Stenger, D. A. *Ann. Biomed. Eng.* **1999**, *27*, 697−711.
(16) Xi, B.; Yu, N.; Wang, X.; Xu, X.; Abassi, Y. A. *Biotechnol. J.* **2008**, *3*, 484−495.
(17) Giaever, I.; Keese, C. R. *Proc. Natl. Acad. Sci. U. S. A.* **1984**, *81*, 3761−3764.
(18) Wegener, J.; Keese, C. R.; Giaever, I. *Exp. Cell Res.* **2000**, *259*, 158−166.
(19) Giaever, I.; Keese, C. R. *Proc. Natl. Acad. Sci. U. S. A.* **1991**, *88*, 7896−7900.
(20) Arndt, S.; Seebach, J.; Psathaki, K.; Galla, H.-J.; Wegener, J. *Biosens. Bioelectron.* **2004**, *19*, 583−594.
(21) Ceriotti, L.; Ponti, J.; Broggi, F.; Kob, A.; Drechsler, S.; Thedinga, E.; Colpo, P.; Sabbioni, E.; Ehret, R.; Rossi, F. *Sens. Actuators, B* **2007**, *123*, 769−778.
(22) Liu, Q.; Yu, J.; Xiao, L.; Tang, J. C. O.; Zhang, Y.; Wang, P.; Yang, M. *Biosens. Bioelectron.* **2009**, *24*, 1305−1310.
(23) Ramis, G.; Martínez-Alarcón, L.; Quereda, J. J.; Mendonça, L.; Majado, M. J.; Gomez-Coelho, K.; Mrowiec, A.; Herrero-Medrano, J. M.; Abellaneda, J. M.; Pallares, F. J.; Ríos, A.; Ramírez, P.; Muñoz, A. *Biomed. Microdevices* **2013**, *15*, 985−995.
(24) Solly, K.; Wang, X.; Xu, X.; Strulovici, B.; Zheng, W. *Assay Drug Dev. Technol.* **2004**, *2*, 363−372.
(25) Xiao, C.; Luong, J. H. T. *Toxicol. Appl. Pharmacol.* **2005**, *206*, 102−112.
(26) Xiao, L.; Hu, Z.; Zhang, W.; Wu, C.; Yu, H.; Wang, P. *Biosens. Bioelectron.* **2010**, *26*, 1493−1499.
(27) Arias, L. R.; Perry, C. A.; Yang, L. *Biosens. Bioelectron.* **2010**, *25*, 2225−2231.
(28) Thakur, M.; Mergel, K.; Weng, A.; Frech, S.; Gilabert-Oriol, R.; Bachran, D.; Melzig, M. F.; Fuchs, H. *Biosens. Bioelectron.* **2012**, *35*, 503−506.
(29) Xie, F.; Xu, Y.; Wang, L.; Mitchelson, K.; Xing, W.; Cheng, J. *Analyst* **2012**, *137*, 1343−1350.
(30) Seeland, S.; Török, M.; Kettiger, H.; Treiber, A.; Hafner, M.; Huwyler, J. *Toxicol. In Vitro* **2013**, *27*, 1109−1120.
(31) Alborzinia, H.; Can, S.; Holenya, P.; Scholl, C.; Lederer, E.; Kitanovic, I.; Wölfl, S. *PLoS One* **2011**, *6*, e19714.
(32) Cao, J.-T.; Zhu, Y.-D.; Rana, R. K.; Zhu, J.-J. *Biosens. Bioelectron.* **2014**, *51*, 97−102.
(33) Tran, T. B.; Cho, S.; Min, J. *Biosens. Bioelectron.* **2013**, *50*, 453−459.

(34) Hong, J.; Kandasamy, K.; Marimuthu, M.; Choi, C. S.; Kim, S. *Analyst* **2011**, *136*, 237−245.
(35) Eker, B.; Meissner, R.; Bertsch, A.; Mehta, K.; Renaud, P. *PLoS One* **2013**, *8*, e57423.
(36) Manz, A.; Graber, N.; Widmer, H. M. *Sens. Actuators, B* **1990**, *1*, 244−248.
(37) Wlodkowic, D.; Khoshmanesh, K.; Sharpe, J. C.; Darzynkiewicz, Z.; Cooper, J. M. *Anal. Chem.* **2011**, *83*, 6439−6446.
(38) Wu, M.-H.; Huang, S.-B.; Lee, G.-B. *Lab Chip* **2010**, *10*, 939−956.
(39) Neuzil, P.; Giselbrecht, S.; Länge, K.; Huang, T. J.; Manz, A. *Nat. Rev. Drug Discovery* **2012**, *11*, 620−632.
(40) Cooksey, G. A.; Elliott, J. T.; Plant, A. L. *Anal. Chem.* **2011**, *83*, 3890−3896.
(41) Wang, L.; Yin, H.; Xing, W.; Yu, Z.; Guo, M.; Cheng, J. *Biosens. Bioelectron.* **2010**, *25*, 990−995.
(42) Meissner, R.; Eker, B.; Kasi, H.; Bertsch, A.; Renaud, P. *Lab Chip* **2011**, *11*, 2352−2361.
(43) Shih, S. C. C.; Barbulovic-Nad, I.; Yang, X.; Fobel, R.; Wheeler, A. R. *Biosens. Bioelectron.* **2013**, *42*, 314−320.
(44) Lei, K. F.; Wu, M.-H.; Hsu, C.-W.; Chen, Y.-D. *Biosens. Bioelectron.* **2014**, *51*, 16−21.
(45) Vergani, M.; Carminati, M.; Ferrari, G.; Landini, E.; Caviglia, C.; Heiskanen, A.; Comminges, C.; Zór, K.; Sabourin, D.; Dufva, M.; Dimaki, M.; Raiteri, R.; Wollenberger, U.; Emnéus, J.; Sampietro, M. *IEEE Trans. Biomed. Circuits Syst.* **2012**, *6*, 498−507.
(46) Zór, K.; Vergani, M.; Heiskanen, A.; Landini, E.; Carminati, M.; Coman, V.; Vedarethinam, I.; Skolimowski, M.; Serrano, A. M.; Kokaia, M.; Moreno, T. R.; Ghio, A.; Svendsen, W. E.; Dimaki, M.; Adamovski, M.; Wollenberger, U.; Sabourin, D.; Ferrari, G.; Raiteri, R.; Sampietro, M.; Dufva, M.; Emnéus, J. *Int. Conf. Miniaturized Syst. Chem. Life Sci., 15th* **2011**, *1*, 1532−1535.
(47) Zór, K.; Heiskanen, A.; Caviglia, C.; Vergani, M.; Landini, E.; Shah, F.; Carminati, M.; Martinez-Serrano, A.; Ramos Moreno, T.; Kokaia, M.; Benayahu, D.; Keresztes, Z.; Papkovsky, D.; Wollenberger, U.; Svendsen, W. E.; Dimaki, M.; Ferrari, G.; Raiteri, R.; Sampietro, M.; Dufva, M.; Emnéus, J. *RSC Adv.* **2014**, DOI: 10.1039/C4RA12632G.
(48) Carter, S. K. *J. Natl. Cancer Inst.* **1975**, *55*, 1265−1274.
(49) Caviglia, C.; Zór, K.; Canepa, S.; Carminati, M.; Muhammad, H. B.; Raiteri, R.; Andresen, T. L.; Heiskanen, A.; Emnéus, J. *Analyst*, submitted for publication, **2015**.
(50) Raymond, E.; Chaney, S. G.; Taamma, A.; Cvitkovic, E. *Ann. Oncol.* **1998**, *9*, 1053−1071.
(51) Graham, J.; Mushin, M.; Kirkpatrick, P. *Nat. Rev. Drug Discovery* **2004**, *3*, 11−12.
(52) Sabourin, D.; Skafte-Pedersen, P.; Søe, M. J.; Hemmingsen, M.; Alberti, M.; Coman, V.; Petersen, J.; Emnéus, J.; Kutter, J. P.; Snakenborg, D.; Jørgensen, F.; Clausen, C.; Holmstrøm, K.; Dufva, M. *J. Lab. Autom.* **2013**, *18*, 212−228.
(53) Skafte-Pedersen, P.; Hemmingsen, M.; Sabourin, D.; Blaga, F. S.; Bruus, H.; Dufva, M. *Biomed. Microdevices* **2012**, *14*, 385−399.
(54) Dimaki, M.; Vergani, M.; Heiskanen, A.; Kwasny, D.; Sasso, L.; Carminati, M.; Gerrard, J. A.; Emneus, J.; Svendsen, W. E. *Sensors* **2014**, *14*, 9505−9521.
(55) Fischer, L. M.; Tenje, M.; Heiskanen, A. R.; Masuda, N.; Castillo, J.; Bentien, A.; Émneus, J.; Jakobsen, M. H.; Boisen, A. *Microelectron. Eng.* **2009**, *86*, 1282−1285.
(56) Caviglia, C.; Carminati, M.; Heiskanen, A.; Vergani, M.; Ferrari, G.; Sampietro, M.; Andresen, T. L.; Emnéus, J. *J. Phys.: Conf. Ser.* **2012**, *407*, 012029.
(57) Kim, L.; Toh, Y.-C.; Voldman, J.; Yu, H. *Lab Chip* **2007**, *7*, 681−694.
(58) Gewirtz, D. A. *Biochem. Pharmacol.* **1999**, *57*, 727−741.
(59) Huo, D.-Q.; Liu, Z.; Hou, C.-J.; Yang, J.; Luo, X.-G.; Fa, H.-B.; Dong, J.-L.; Zhang, Y.-C.; Zhang, G.-P.; Li, J.-J. *Chin. J. Anal. Chem.* **2010**, *38*, 1357−1365.
(60) Jedrych, E.; Flis, S.; Sofinska, K.; Jastrzebski, Z.; Chudy, M.; Dybko, A.; Brzozka, Z. *Sens. Actuators, B* **2011**, *160*, 1544−1551.
(61) Raymond, E.; Faivre, S.; Chaney, S.; Woynarowski, J.; Cvitkovic, E. *Mol. Cancer Ther.* **2002**, *1*, 227−235.
(62) William-Faltaos, S.; Rouillard, D.; Lechat, P.; Bastian, G. *Anticancer Res.* **2006**, *26*, 2093−2099.
(63) Rixe, O.; Ortuzar, W.; Alvarez, M.; Parker, R.; Reed, E.; Paull, K.; Fojo, T. *Biochem. Pharmacol.* **1996**, *52*, 1855−1865.
(64) Arango, D.; Wilson, A. J.; Shi, Q.; Corner, G. A.; Arañes, M. J.; Nicholas, C.; Lesser, M.; Mariadason, J. M.; Augenlicht, L. H. *Br. J. Cancer* **2004**, *91*, 1931−1946.
(65) Faivre, S.; Chan, D.; Salinas, R.; Woynarowska, B.; Woynarowski, J. M. *Biochem. Pharmacol.* **2003**, *66*, 225−237.
(66) Kratz, F.; Müller, I. A.; Ryppa, C.; Warnecke, A. *ChemMedChem* **2008**, *3*, 20−53.
(67) Kaasgaard, T.; Andresen, T. L. *Expert Opin. Drug Delivery* **2010**, *7*, 225−243.
(68) Choi, K. Y.; Swierczewska, M.; Lee, S.; Chen, X. *Theranostics* **2012**, *2*, 156−178.
(69) Hatakeyama, H.; Akita, H.; Kogure, K.; Oishi, M.; Nagasaki, Y.; Kihira, Y.; Ueno, M.; Kobayashi, H.; Kikuchi, H.; Harashima, H. *Gene Ther.* **2007**, *14*, 68−77.